

Inversion of stellar fundamental parameters from Espadons and Narval high-resolution spectra[★]

F. Paletou, T. Böhm, V. Watson, and J.-F. Trouilhet

¹ Université de Toulouse, UPS-Observatoire Midi-Pyrénées, IRAP, Toulouse, France

² CNRS, Institut de Recherche en Astrophysique et Planétologie, 14 av. E. Belin, F-31400 Toulouse, France
e-mail: fpaletou@irap.omp.eu

Received August 4, 2014; accepted November 10, 2014

ABSTRACT

The general context of this study is the inversion of stellar fundamental parameters from high-resolution Echelle spectra. We aim indeed at developing a fast and reliable tool for the post-processing of spectra produced by Espadons and Narval spectropolarimeters. Our inversion tool relies on principal component analysis. It allows reduction of dimensionality and the definition of a specific metric for the search of nearest neighbours between an observed spectrum and a set of observed spectra taken from the Elodie stellar library. Effective temperature, surface gravity, total metallicity and projected rotational velocity are derived. Various tests presented in this study, and done from the sole information coming from a spectral band centered around the Mg I b-triplet and with spectra from FGK stars are very promising.

Key words. Methods: data analysis – Stars: fundamental parameters – Astronomical databases: miscellaneous

1. Introduction

This study is concerned with the inversion of fundamental stellar parameters from the analysis of high-resolution Echelle spectra. Hereafter, we shall focus indeed on data collected since 2006 with the Narval spectropolarimeter mounted at the 2-m aperture *Télescope Bernard Lyot* (TBL) telescope located at the summit of the *Pic du Midi de Bigorre* (France) and, since 2005 with the Espadons spectropolarimeter mounted at the 3.6-m aperture CFHT telescope (Hawaii). We investigate, in particular, the capabilities of the principal component analysis (hereafter PCA) for setting-up a fast and reliable tool for the inversion of stellar fundamental parameters from these high-resolution spectra.

The inversion of stellar fundamental parameters for each target that was observed with both Narval and Espadons spectropolarimeters constitutes an essential step towards: (i) the further post-processing of the data like e.g., the extraction of polarimetric signals (see e.g., Paletou 2012 and references therein) but also (ii) the exploration, or data mining, of the full set of data accumulated over the last 8 years now. In Section 2, we briefly describe the actual content of such a database¹.

PCA have been used for stellar spectral classification since Deeming (1964). It has been in use since, and more recently for the purpose of the *inversion* of stellar fundamental parameters from the analysis of spectra of various resolutions. It is however most often used *together* with artificial neural networks (see e.g., Bailer-Jones 2000; Re Fiorentin et al. 2007). PCA is used there

for reducing the dimensionality of the spectra before attacking a multi-layer perceptron which, in turns, allows to link input data to stellar parameters.

Our usage of PCA for such an inversion process is strongly influenced by the one routinely made in *solar* spectropolarimetry during the last decade after the pioneering work of Rees et al. (2000). Very briefly, the reduction of dimensionality allowed by PCA is directly used for building a specific metric from which a nearest neighbour(s) search is done between an observed data set and the content of a “training database”. The latter can be made of synthetic data generated from input parameters properly covering the *a priori* range of physical parameters expected to be deduced from the observations themselves. A quite similar use of PCA was also presented for classification and redshift of galaxies estimation by Cabanac et al. (2002). However, in this study we shall use *observed* spectra from the Elodie stellar library, as our data set of reference (Prugniel et al. 2007). Such spectra have been, for instance, used in a recent study related to the determination of atmospheric parameters of FGKM stars in the Kepler field (Molenda-Żakowicz et al. 2013). Fundamental elements of our method are exposed in Section 3. Its main originality relies also on the simultaneous inversion of the effective temperature T_{eff} , the surface gravity $\log g$, the metallicity [Fe/H] and the projected rotational velocity $v \sin i$ directly and only from a specific spectral band extracted from the full range covered by Espadons and Narval.

As compared to alternative methods such as χ^2 fitting to a library of (synthetic) spectra, as done by Munari et al. (2005) for the analysis of the RAVE survey, for instance, the main advantages of PCA are in the reduction of dimensionality – a critical issue when dealing with high-resolution spectra also covering a very large bandwidth – which allows a very fast processing of the data, and in the “denoising” of the original data (see e.g., Bailer-Jones et al. 1998 or Paletou 2012 in another context though).

[★] Based on observations obtained at the *Télescope Bernard Lyot* (TBL, *Pic du Midi*, France), which is operated by the *Observatoire Midi-Pyrénées*, *Université de Toulouse*, *Centre National de la Recherche Scientifique* (France) and the *Canada-France-Hawaii Telescope* (CFHT) which is operated by the *National Research Council of Canada*, *CNRS/INSU* and the *University of Hawaii* (USA).

¹ polabase.irap.omp.eu

It also differs from another projection method such as Matisse which uses specific projection vectors attached, say, to each stellar parameter to be inverted (Recio-Blanco et al. 2006). In that frame, these vectors are derived after assuming that they are linear combinations of every “individual” belonging to a learning database of synthetic spectra.

In this study we restrict ourselves, on purpose, to a spectral domain ranging from 500 to 540 nm, that is around the Mg I b-triplet lines. The main argument in favour of this spectral domain lies in the fact that spectral lines of this triplet are excellent surface gravity indicators (e.g., Cayrel & Cayrel 1963, Cayrel de Strobel 1969), $\log g$ being at the same time the most difficult parameter to retrieve from spectral data. It is also a spectral domain devoid of telluric lines. More recently, Gazzano et al. (2010) performed a convincing spectral analysis of Flames/Giraffe spectra working with a similar spectral domain. However, in our study we shall use *observed* spectra as training database for our PCA-based method of inversion.

Preliminary tests, done with the inversion of spectra taken from the so-called S⁴N survey (Allende Prieto et al. 2004), are discussed in Section 4. Finally, we proceed with the inversion of 140 spectra of FGK stars from POLARBASE for which fundamental parameters are already available from the so-called SPOCS catalogue of Valenti & Fisher (2005).

2. Sources of data

Our reference spectra are taken from the Elodie stellar library (Prugniel et al. 2007, Prugniel & Soubiran 2001). They are publicly available² and fully documented. An important information concerns the wavelength coverage of Elodie spectra, which is about 390–680 nm. This, unfortunately, prevents us from doing tests in the spectral domain at the vicinity of the infrared triplet of Ca II for instance (see e.g., Munari 1999 for a detailed case concerning this spectral range). We used also the high-resolution spectra at $\mathcal{R} \sim 42\,000$.

First tests of our method were done with stellar spectra coming from the *Spectroscopic Survey of Stars in the Solar Neighbourhood*, aka. S⁴N survey (Allende Prieto et al. 2004). They are also publicly³ available and fully documented. The wavelength coverage is 362–1044 nm (McDonald Observatory, 2.7-m telescope) or 362–961 nm (La Silla, 1.52-m telescope) and spectra have resolution $\mathcal{R} \sim 50\,000$.

However, our main purpose is the inversion of stellar parameters from high-resolution spectra coming from Narval and Espadons spectropolarimeters. Such data is now available from the *public* database POLARBASE (Petit et al. 2014). Narval is a state-of-the-art spectropolarimeter operating in the 380–1000 nm spectral domain, with a spectral resolution of 65 000 in its polarimetric mode. It is an improved copy, adapted to the 2-m TBL telescope, of the Espadons spectropolarimeter, in operations since 2004 at the 3.6-m aperture CFHT telescope.

POLARBASE is operational since 2013. It is at the present time the largest on-line archive of high-resolution polarization spectra. It hosts data that were taken at the 3.6-m CFHT telescope since 2005 and with the 2-m TBL telescope since 2006. So far, more than 180 000 independent spectra are available, for more than 2 000 distinct targets all over the Hertzsprung-Russell diagram. More than 30 000 *polarized* spectra are also available, mostly for *circular* polarization. Linear polarization data are very seldom still and amount to a about 2% of the available data.

² see: <http://atlas.obs-hp.fr/elodie/>

³ hebe.as.utexas.edu/s4n/

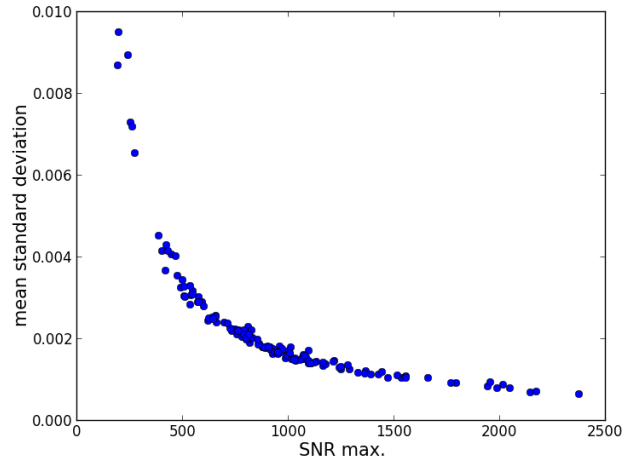


Fig. 1. Typical domain of variation of the noise level associated with the Espadons-Narval spectra we shall process. The mean standard deviation of noise per pixel, for the wavelength range around the b-triplet of Mg I is displayed here vs. the maximum signal to noise ratio of the full spectra.

At the present time, the PolarBase database provides no more than Stokes I or V/I_c spectra calibrated in wavelength. Stokes I data are either normalized to the local continuum or not. We have however plans to propose higher-level data, such as pseudo-profiles resulting from line addition and/or least-squares deconvolution (see e.g., Paletou 2012), activity indexes as well as stellar fundamentals parameters. The latter’s knowledge, besides being obviously interesting by itself, is also indispensable to any accurate further post-processing of these high-resolution spectra. These spectra are also generally bearing high signal-to-noise ratios, as can be seen in Fig. (1). Indeed Stokes I spectra we have been using result from the combination of 4 successive exposures, each of them carrying 2 spectra of orthogonal polarities generated by a *Savart* plate-type analyser. This procedure of double so-called “beam-exchange” measurement is indeed meant for the purpose of extracting (very) weak polarization signals (see e.g., Semel et al. 1993).

3. PCA-based inversion

Our PCA-based inversion tool is strongly inspired by magnetic and velocity field inversion tools which have been developed during the last decade to diagnose solar spectropolarimetric data (see e.g., Rees et al. 2000). Improvements of this method have been recently exposed by Casini et al. (2013) for instance. Hereafter, we describe its main characteristics, in the particular context of our study.

3.1. The training database

Our training database was created after the Elodie stellar spectral library (Prugniel et al. 2007, Prugniel & Soubiran 2001; see also Vizier@CDS catalogue III/251). Stellar parameters associated with each spectra have been extracted by us from the CDS, using resources from the Python package *astroquery*⁴, in particular its components allowing to query Vizier catalogues.

⁴ astroquery.readthedocs.org

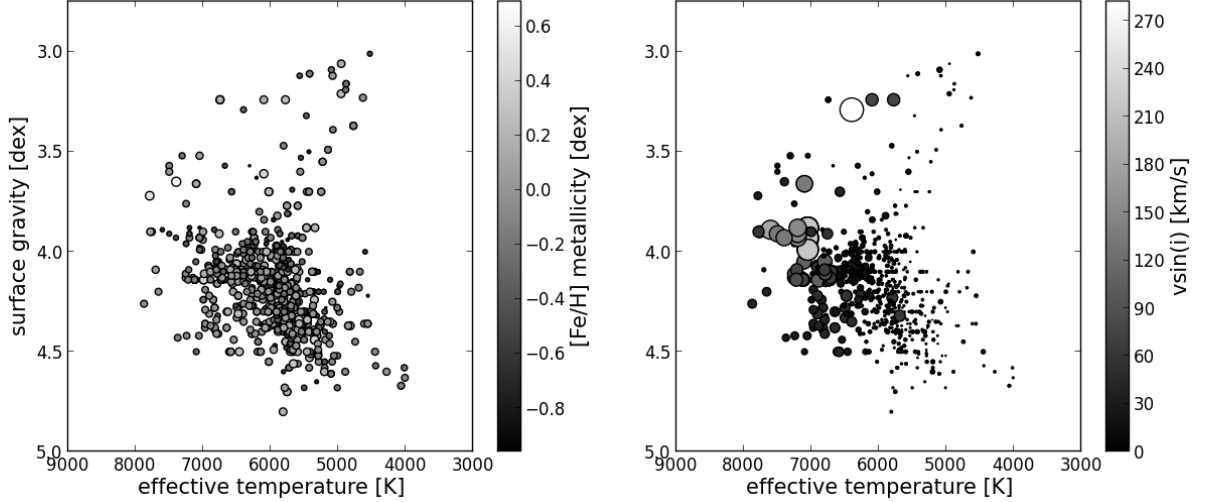


Fig. 2. Graphical summary of the coverage in stellar parameters corresponding to the content of our Elodie spectra training database (for FGK stars). Note that we adopted values of $v\sin i$ from Vizier@CDS catalogue III/244 (Głebocki & Gnaniński 2005). Size and color of each dot are proportional to either $[\text{Fe}/\text{H}]$ (left) or $v\sin i$ (right).

We had, however, to complement these informations with a value of the projected rotational velocity for each object/spectra of our database. To do so, we have been querying the catalogue of stellar rotational velocities of Głebocki & Gnaniński (2005, also Vizier@CDS catalogue III/244⁵). Note also that we removed all objects for which we could not find a value of $v\sin i$ in this catalogue.

Since our preliminary tests concerns the inversion of the S⁴N survey as well as objects common between the content of POLARBASE and the one of the so-called Spocs catalogue (Valenti & Fisher 2005), we limited ourselves to such spectra for which T_{eff} lies between 4 000 and 8 000 K, $\log g$ is greater than 3.0 dex and $[\text{Fe}/\text{H}]$ is greater than -1.0 dex. We also had to reject a few Elodie spectra which we found improperly corrected for radial velocity and therefore misaligned in wavelength with respect to the other spectra. The various coverage in stellar parameters coming along the finally 905 selected spectra are summarized in Figs. (2).

Finally, following Muñoz Bermejo et al. (2013; see their §2.1) we adopted the same renormalization procedure, homogeneously, for the whole set of Elodie spectra making our training database. It is an iterative method consisting in two main steps. The first stage consists in fitting the normalized flux in the spectral bandwidth of interest by a high-order (8-th) polynomial. Then we compute $D(\lambda)$ i.e, the difference between the initial spectra and the polynomial fit, as well as its mean \bar{D} and standard deviation σ_D . We reject these wavelengths such that $(D - \bar{D})$ are either beyond $-0.5\sigma_D$ or above $3\sigma_D$. This scheme is iterated 10 times, which guarantees that we properly extract the continuum envelope of the initial spectra. Finally, we use the remaining flux values to renormalize the initial spectra. As shows Fig. (3), this concerns relatively small corrections of the continuum level, never exceeding a few percents. As mentioned earlier by Muñoz Bermejo et al. (2013), this procedure may be arguable, but we found it satisfactory and it was consistently applied to all the spectra we used.

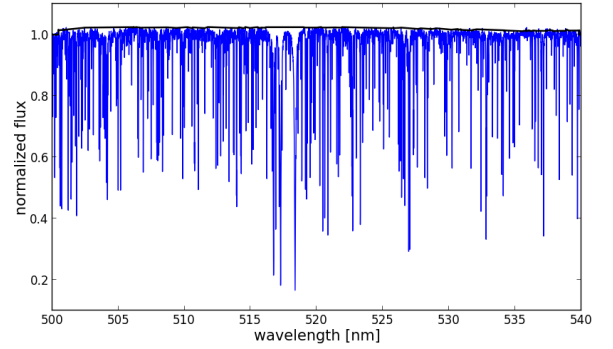


Fig. 3. A typical example of the continuum level fit (strong dark line) on top of the original spectrum still bearing small normalization errors to be corrected for.

3.2. Reduction of dimensionality

Espadons and Narval spectropolarimeters typically provide of the order of 250 000 flux measurements vs. wavelength across a spectral range spanning from about 380 to 1000 nm, for each spectra. Hereafter we shall only consider spectra obtained in the polarimetric mode at a resolvance of $\mathcal{R} \sim 65\,000$. Indeed, one of our main objective is that stellar parameters derived from Stokes I spectra can be directly used for the further post-processing of the multi-line *polarized* spectra which is obtained simultaneously (see e.g., Paletou 2012 and references therein).

In this study, we adopt a first reduction of dimensionality by restricting the spectral domain from which we shall invert stellar parameters to the vicinity of the Mg I b-triplet that is, for wavelengths ranging from 500 to 540 nm. The presence of good surface gravity indicators like the strong lines of the b-triplet of Mg I ($\lambda\lambda$ 516.75, 517.25 and 518.36 nm) as well as several other metallic lines in their neighbourhood, and the absence of telluric lines in this spectral domain are the main arguments we used. Considering this, the matrix \mathcal{S} representing our training database sizes like $N_{\text{spectra}} = 905$ by $N_{\lambda} = 8\,000$.

⁵ We had to correct the value of 25 km s^{-1} given for HD 16232, significantly underestimated vs. alternative determinations (with a median of 40 km s^{-1})

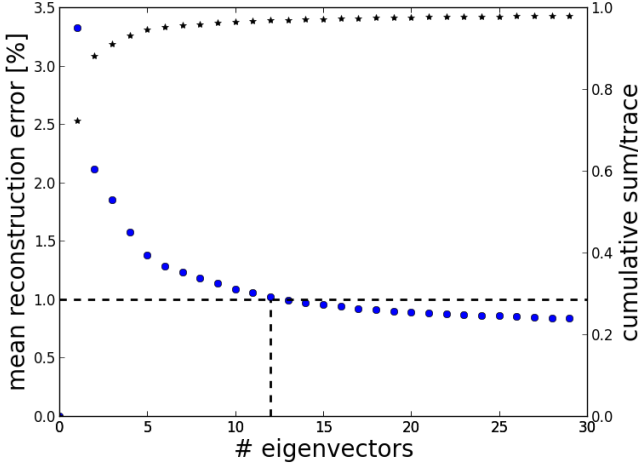


Fig. 4. Reconstruction error as a function of the number of eigenvectors used for the computation of the projection coefficients p . The mean reconstruction error gets below 1% (with a standard deviation of 0.4%) after rank 12. The rightside scale is for the cumulative sum of the ordered eigenvalues normalized to their sum (\star).

Next, we compute the eigenvectors $e_k(\lambda)$ of the variance-covariance matrix defined as

$$C = (S - \bar{S})^T \cdot (S - \bar{S}), \quad (1)$$

where \bar{S} is the mean of S along the N_{spectra} -axis. Therefore C is a $N_\lambda \times N_\lambda$ matrix. In the framework of principal component analysis, reduction of dimensionality is achieved by representing the original data by a limited set of projection coefficients

$$p_{jk} = (S_j - \bar{S}) \cdot e_k, \quad (2)$$

with $k_{\text{max}} \ll N_\lambda$. In what follows for the processing of all observed spectra, we shall adopt $k_{\text{max}} = 12$.

The most frequent argument supporting the choice of k_{max} relies on the accuracy achieved for the reconstruction of the original set of S_i 's from a limited set of eigenvectors (see e.g., Rees et al. 2000 or Muñoz Bermejo et al. 2013). In the present case, we display in Fig. (4) the mean reconstruction error

$$E(k_{\text{max}}) = \left\langle \left| \frac{1 \bar{S} + \sum_{k=1}^{k_{\text{max}}} p_{jk} e_k - S_j}{S_j} \right| \right\rangle, \quad (3)$$

as a function of the maximum number of eigenvectors considered for the computation of the projection coefficients p . It is noticeable in Fig. (4) that this reconstruction error is better than 1% for $k_{\text{max}} \geq 12$. Also, at the same rank, an alternative estimator like the cumulative sum of the ordered eigenvalues normalized to their sum becomes larger than 0.95.

To conclude this part, we display in Fig. (5) the 12 eigenvectors that we shall use further.

3.3. Nearest neighbour(s) search

The above described reduction of dimensionality allows one to perform a fast and reliable inversion of observed spectra, once the latter have been: (i) corrected for the wavelength shift vs. the spectra in our database, because of the radial velocity of

Table 1. Bias and standard deviation of the differences between *inverted* Elodie spectra and its initial stellar parameters of reference T_{eff} (K), $\log g$ and $[\text{Fe}/\text{H}]$ (dex) and $v \sin i$ (km s^{-1}). At each step, the Elodie spectra being processed was removed from the training database.

Parameter	T_{eff}	$\log g$	$[\text{Fe}/\text{H}]$	$v \sin i$
bias	0.78	0.02	0.005	0.07
σ	170	0.16	0.11	6.84

the target, (ii) continuum-renormalized as accurately as possible, (iii) degraded in spectral resolution to be comparable to the $\mathcal{R} \sim 42\,000$ resolvance of the Elodie spectra we use and, finally (iv) resampled in wavelength as the collection of Elodie spectra. We shall come back to these various stages in the next section. However once these tasks have been achieved, the inversion process is the following.

Let $O(\lambda)$ the observed spectrum made comparable to Elodie ones. We now compute the set of projection coefficients

$$o_k = (O - \bar{S}) \cdot e_k. \quad (4)$$

The nearest neighbour search is therefore done by seeking the minimum of the squared *Euclidian* distance

$$d_j^{(O)} = \sum_{k=1}^{k_{\text{max}}} (o_k - p_{jk})^2, \quad (5)$$

where j spans the number, or a limited number if any *a priori* is known about the target, of distinct reference spectra in the training database. In practice, we do not limit ourselves to the nearest neighbour search, although it already provides a relevant set of stellar parameters. Because PCA-distances between several neighbours may be of the same order, we adopted a simple procedure which consists in considering *all* neighbours in a domain

$$\min(d_j^{(O)}) \leq d_j^{(O)} \leq 1.2 \times \min(d_j^{(O)}), \quad (6)$$

and derive stellar parameters as the (simple) mean of each set of parameters $\{T_{\text{eff}}; \log g; [\text{Fe}/\text{H}]; v \sin i\}$ characterising this set of nearest neighbours (A. López Ariste, private communication). We did not notice significant changes in the results either for a smaller range of PCA-distances or when adopting e.g., distance-weighted mean parameters. This point will be discussed again in the forthcoming sections.

3.4. Internal error

In order to characterize our inversion method, we have been inverting stellar parameters T_{eff} , $\log g$, $[\text{Fe}/\text{H}]$ and $v \sin i$ for every spectra (905) constituting the training database. However, at each step we removed the spectra being processed from the database (and then recomputed the eigenvalues and eigenvectors of the new variance-covariance matrix).

To summarize this analysis, we give in Table 1 internal errors, σ , measured for each inverted stellar parameter. The disappointing result on $v \sin i$ mainly comes from a suspicious scatter of results for these objects having large $v \sin i$, typically beyond 100 km s^{-1} . However, for our tests with $S^4\text{N}$ and POLARBASE data, we did not have to deal with objects having $v \sin i$ beyond 80 km s^{-1} (see next sections).

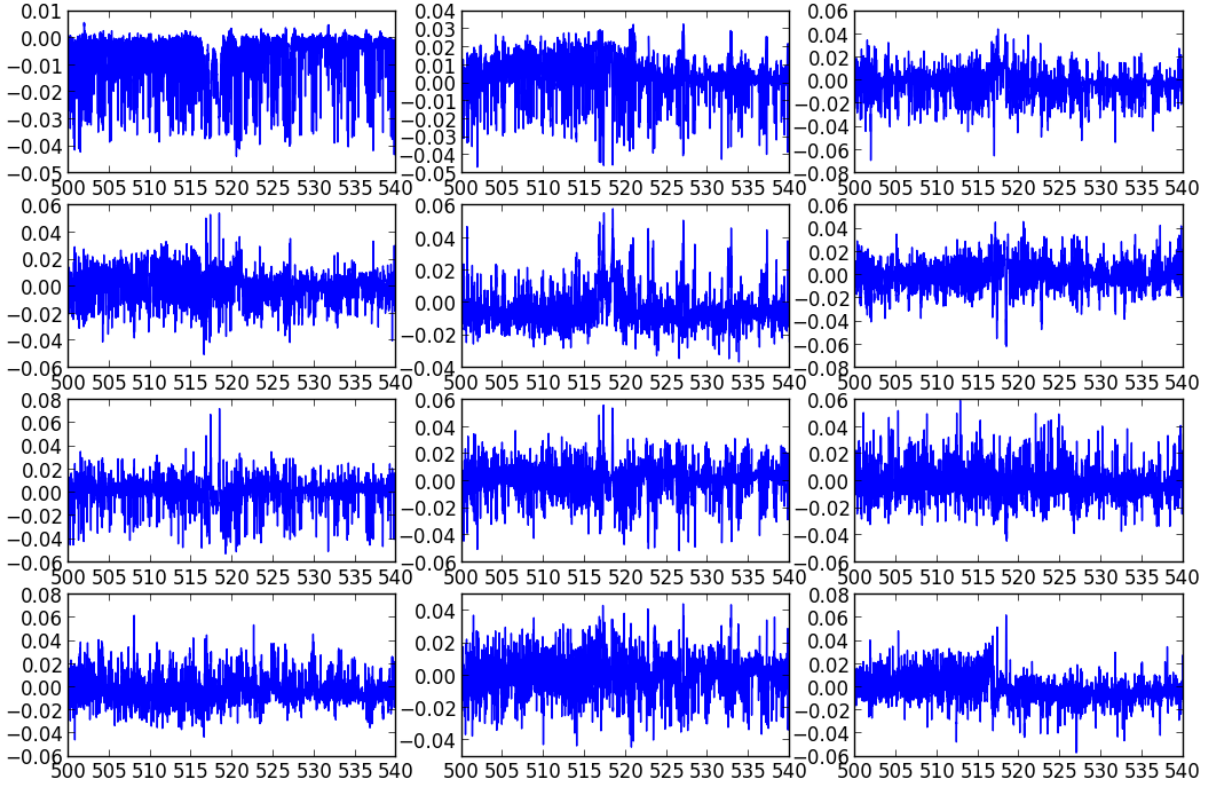


Fig. 5. From top left to bottom right, the 12 eigenvectors used in our inversion method. Each of them is displayed vs. the same wavelength scale in nm.

4. Inversion of S⁴N spectra

A convincing test of our method would be to invert high-resolution spectra which were gathered in the frame of the so-called *Spectroscopic Survey of Stars in the Solar Neighbourhood* (aka. S⁴N, Allende Prieto et al. 2004)

We selected only these S⁴N spectra for which *all* three parameters $\{T_{\text{eff}}; \log g; [\text{Fe}/\text{H}]\}$ have been determined by Allende Prieto et al. (2004). We used the same reference catalogue as the one used for the Elodie spectra to add a $v \sin i$ value to each spectra (see e.g., Paletou & Zolotukhin 2014). Since they were acquired at a higher spectral resolution than Elodie ones, we adapted each spectra to the latter resolution $\mathcal{R} \sim 42\,000$ using an appropriate Gaussian filter. Finally we applied to all spectra the same renormalization procedure as the one also applied to our Elodie spectra database.

We identified 49 objects in common between S⁴N and our sample of 905 objects taken from the Elodie Stellar Library. Using respective catalogue values for effective temperature T_{eff} , surface gravity $\log g$ and metallicity $[\text{Fe}/\text{H}]$ we could easily estimate bias and standard deviations between the two distinct estimates, for each stellar parameter. Results are summarized in Table 2.

This should be now compared to the results of our *inversion* of 104 S⁴N spectra using our Elodie training database for PCA. They are summarized, for each stellar parameters including $v \sin i$ though, both in Fig. (6) and in Table 3 (where we also detail specific values for, respectively, the inversion of the spectra of the

Table 2. Bias and standard deviation of the absolute differences between *reference* stellar parameters T_{eff} (K), $\log g$ (dex) and $[\text{Fe}/\text{H}]$ (dex) retrieved respectively from the S⁴N and the Elodie catalogues, for the 49 objects in common between our data samples.

Parameter	T_{eff}	$\log g$	$[\text{Fe}/\text{H}]$
bias	-66	0.16	0.006
σ	84	0.14	0.08

49 objects in common between S⁴N and our Elodie sample, and the 55 remaining objects). Bias and dispersions, especially conspicuous for $\log g$, measured after our inverted parameters appear to be quite direct imprints of the discrepancies already put in evidence, by the direct comparison between respective reference values for objects in common between the two samples. However, taking into account that our inversion relies *only* on spectroscopic information, moreover on a limited (but relevant) spectral band, we find our approach satisfactory for our purpose.

Our method allows also a reliable and *direct* inversion of the projected rotational velocity $v \sin i$ of stars, without any other limitation than the one coming from the limit in $v \sin i$ attached to the identified values for spectra present in our Elodie training database – see e.g., Figs. (2). Using synthetic spectra (computed for hypothetical non-rotating stars) Gazzano et al. (2010) study was, for instance, limited to stars having a $v \sin i$ lower than about 11 km s^{-1} . In our case, we retrieve accurately $v \sin i$ values up the

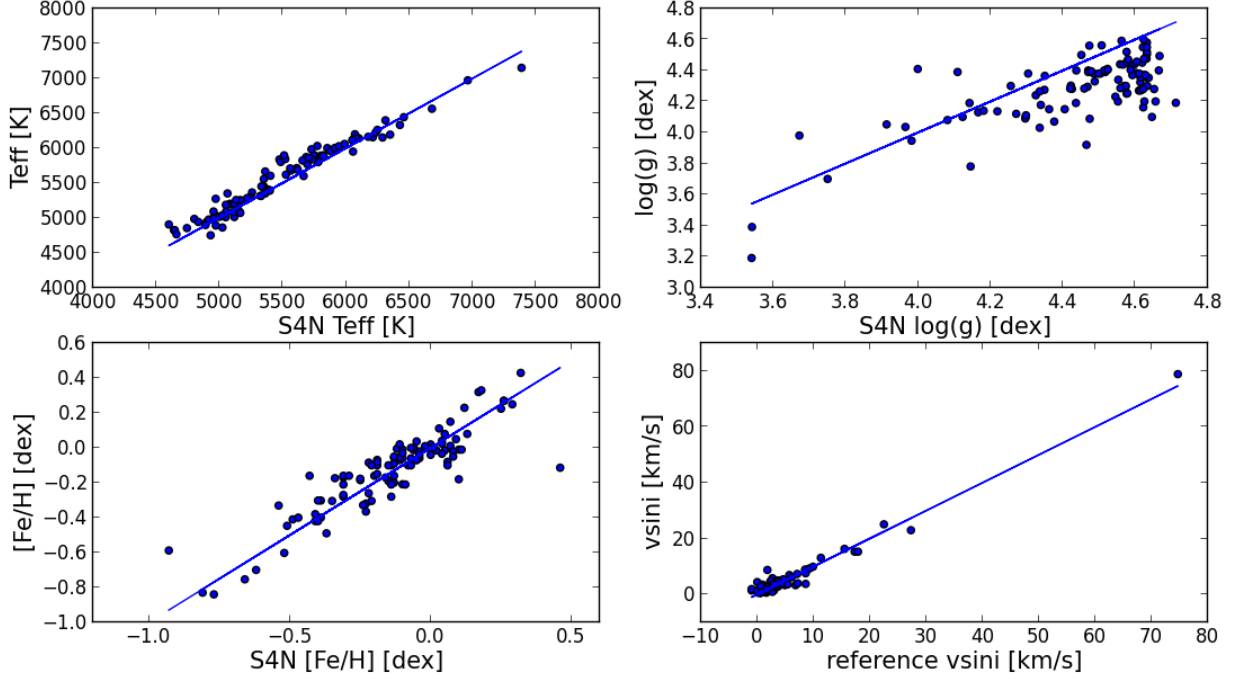


Fig. 6. Stellar fundamental parameters inverted from the analysis of S⁴N spectra, using our PCA-Elodie method vs. their S⁴N catalogue values of reference (except for $v_{\text{sin}i}$ – see text). Respective bias and standard deviation deduced from the analysis of the difference between inverted and catalogue/reference parameters are: (-74 ; 115) for T_{eff} , (0.16 ; 0.16) for $\log g$ and (-0.01 ; 0.11) for [Fe/H]. For $v_{\text{sin}i}$ values, for which the source of data is not the S⁴N catalogue however, we find (-0.36 ; 1.61).

Table 3. Bias and standard deviation of the absolute differences between *inverted* and reference stellar parameters T_{eff} (K), $\log g$ and [Fe/H] (dex) and $v_{\text{sin}i}$ (km s⁻¹), for our sample of 104 S⁴N spectra – see also Fig. (6).

Parameter	T_{eff}	$\log g$	[Fe/H]	$v_{\text{sin}i}$
bias	-74	0.16	-0.01	-0.36
σ	115	0.16	0.11	1.61
49 objects in common				
bias	-62	0.16	0.001	-0.16
σ	82	0.16	0.08	0.67
55 objects not in common				
bias	-85	0.15	-0.02	-0.55
σ	138	0.17	0.13	2.10

most extreme case of $\sim 80 \text{ km s}^{-1}$ in our sample i.e., the high-proper motion FIV star HIP 77952⁶ i.e., fast rotators for which usual synthetic models are unsatisfactory.

Another advantage of our method is that nearest neighbour(s) are also identifiable as *objects* i.e., other stars. In that sense, our method can also be seen as relevant from *classification*. For instance, considering the only objects in common between our S⁴N and our Elodie spectra/objects sample, in 75% of the cases the very nearest neighbour is another spectra of the *same* object and, for the remainder, conditions expressed in Eq. (6) guarantee that the same object spectra belongs to the set of nearest neighbours.

⁶ Note that for this object, one can identify 5 estimates of $v_{\text{sin}i}$ from Vizier@CDS ranging from 70 to 90 km s⁻¹, but whose median value of 75 km s⁻¹ agrees very well with our own estimate.

5. Inversion of PolarBase spectra

Hereafter we shall first discuss details about which kind of conditioning have to be applied to POLARBASE spectra in order to be made comparable to our Elodie-based training database. Then we shall discuss the inversion of spectra of the Sun taken on reflection over the Moon surface at the TBL telescope, and finally inversions of 140 spectra from FGK objects in common with the sample studied by Valenti & Fischer (2005).

5.1. Conditioning of PolarBase spectra

The first and obvious task to perform on *observed* spectra is to correct for their wavelength shift vs. Elodie spectra which are found already corrected for radial velocity (v_{rad}). The radial velocity of the target at the time of the observation is deduced from the centroid, in a velocity space, of the pseudo-profile resulting from the “addition” (see e.g., Paletou 2012) of the three spectral lines of the Ca II infrared triplet whose rest wavelengths are, respectively, 849.802, 854.209 and 866.214 nm. Note that this can be done with any other set of spectral line supposed to be *a priori* present in the spectra we want to process. One of the advantages of the Ca II infrared triplet is its “persistence” for spectral types ranging from A to M. Once v_{rad} is known, the observed profile is set on a new wavelength grid, at rest.

We could check, using a solar spectra (see also the next section) that v_{rad} should be known to an accuracy of the order of $\delta v/4$ with $\delta v = c/R$ i.e., about 1.15 km s^{-1} with our Espadons-Narval data. Beyond this value, estimates of T_{eff} and $v_{\text{sin}i}$ first, start to be significantly affected by the misalignment of the observed spectral lines with those of the spectra of the train-

Table 4. Bias and standard deviation of the absolute differences between stellar parameters T_{eff} (K), surface gravity $\log g$ and metallicity $[\text{Fe}/\text{H}]$ (dex) and projected rotational velocity $v \sin i$ (km s^{-1}) obtained respectively from the Spocs catalogue of Valenti & Fischer (2005, reference values) and our inversion method using Elodie spectra.

Parameter	T_{eff}	$\log g$	$[\text{Fe}/\text{H}]$	$v \sin i$
bias	23	0.10	0.02	-0.04
σ	115	0.19	0.10	1.68

ing database. Indeed, the neighbourhood identified by our PCA-based approach can change quite dramatically because of such a spectral misalignment.

A second step consists in adapting the resolution of the initial spectra, about $\mathcal{R} \sim 65\,000$ in the polarimetric mode, to the one of the training database spectra i.e., $\mathcal{R} \sim 42\,000$. This is done by convolving the initial observed profile by a Gaussian profile of adequate width. Then we resample the wavelength grid down to the one common to all reference spectra, and we interpolate the original spectra onto the new wavelength grid. Finally, we apply the same renormalization procedure as already described in §3.1, for consistency.

5.2. Solar spectra observed with Narval

First tests of our inversion method with POLARBASE data were performed using solar spectra observed by the 2-m aperture TBL telescope by reflection over the surface of the Moon in March and June 2012.

Using the very same training database as the one used for the tests done with $S^4\text{N}$ data, we could identify as “nearest neighbour” star to the Sun HD 186427 (aka. 16 Cyg B). It is indeed a G3V planet-hosting star often identified as being a solar twin (see e.g., Porto de Mello et al. 2014). Its stellar fundamental parameters are: $T_{\text{eff}}=5757$ K, $\log g=4.35$ dex, $[\text{Fe}/\text{H}]=0.06$ and $v \sin i \sim 2.18$ km s^{-1} (see also Tucci Maia et al. 2014, for a recent determination of these parameters). The other nearest neighbour we could identify is HD 29150, a star whose main parameters are: $T_{\text{eff}}=5733$ K, $\log g \sim 4.35$ dex (Lee et al. 2011, from Simbad@CDS query), $[\text{Fe}/\text{H}]=0.0$ and $v \sin i \sim 1.8$ km s^{-1} .

Taking into consideration this neighbourhood, in the PCA-sense, we thus derive quite satisfactory estimates for effective temperature $T_{\text{eff}}=5745$ K, surface gravity $\log g=4.35$ dex, a metallicity of $[\text{Fe}/\text{H}]=0.03$ and $v \sin i \sim 2$ km s^{-1} typical of the (very) slowly rotating Sun, as observed by reflection over the Moon surface with the Narval@TBL spectropolarimeter.

This is quite consistent with the test consisting in inverting the Sun spectra taken from the Elodie stellar library, but *not* a member of our training database. In such a case, we recover neighbours 16 Cyg B and HD 29150 plus the additional HD 146233 (aka. 18 Sco) and HD 42807, a RS CVn star of G2V type, also very similar to the Sun indeed.

5.3. Other FGK stars

We identified in the present content of POLARBASE 140 targets which are also identified in the Spocs catalogue. For our next tests of our method, we selected these spectra having the best signal to noise ratio for every object. Typical values were already given in Fig. (1).

Results and characterization of our inversion are given both in Table 4 and, with more details in Fig. (7). The latter figure

also gives an idea about the range of variations of parameters which are expected for the set of spectra/objects being studied here. Overall figures are quite similar to the ones obtained with the $S^4\text{N}$ although bias values for T_{eff} and $\log g$ are smaller with Spocs data.

5.3.1. Effective temperature

This standard deviation on the differences between our values and Spocs reference ones is the same as the one we could evaluate using $S^4\text{N}$ spectra (see. Table 3). However the bias value of 23 K is much smaller for this sample of objects and POLARBASE spectra. We note also that the most important dispersion is for the coolest objects of our sample, for T_{eff} about 5000 K.

A more detailed inspection of outliers in effective temperature, taking into account alternative and more recent estimates of T_{eff} than the one adopted from Spocs, reveals that the most extreme ΔT_{eff} we identified are quite often overestimated. This is for instance the case for the K1V star LHS 44 for which a recent determination by Maldonado et al. (2012) is +200 K from the one of Valenti & Fischer (2005) and only 140 K from ours. Another effect may also come from new estimates of parameters for Elodie objects themselves, an issue we shall discuss hereafter.

Our estimates of effective temperature from spectropolarimetric data are however already satisfactory for being used in the selection of a proper “mask” (i.e., at least a list of spectral lines) that will be, in turn, used for the further extraction of polarized signatures.

5.3.2. Surface gravity

It is well-known that surface gravity is the most difficult parameter to get from the analysis of spectroscopic data. The most conspicuous outliers show quite easily on the $\log g$ subplot in Fig. (7). In the “top-3” of them showing $\Delta \log g \sim 0.5$ dex or above, we find: EK Dra, LTT 8785 and HD 22918. Concerning EK Dra, our estimate of $\log g \sim 3.6$ dex is way too low as compared to (seldom) values found in the litterature (~ 4.5 dex). This may be compensated by the fact that its identified nearest neighbour star is the G2IV *subgiant* HD 126868 (aka. 105 Vir) for which $\log g = 3.6$ dex in the Elodie catalogue, although a value of 3.9 dex is reported elsewhere (see e.g., the PASTEL catalogue: Soubiran et al. 2010). For LTT 8785 and HD 22918, examination of alternative estimates for $\log g$ (e.g., Massarotti et al. 2008; Jones et al. 2011) show that Spocs values may have been slightly overestimated. Besides, the surface gravity ($\log g \sim 3.23$) of the nearest neighbour (and the same object in both cases) HD 42983 may have been underestimated. An inspection of Vizier@CDS for this object indicates 4 different estimates ranging from 3.23 to 3.6 with a median value of 3.5. Taking this into account, $\Delta \log g$ does not exceed 0.2 dex between our inverted values and reference ones, which is satisfactory.

5.3.3. Metallicity

Let us now inspect our results for metallicity. First of all, we included into our sample LHS 44 which $[\text{Fe}/\text{H}]=-1.16$ according to Valenti & Fischer (2005), a value *a priori* excluded from our working range. But even though, our inversion method points at these objects in our sample bearing the lowest $[\text{Fe}/\text{H}]$ values. Then by decreasing order of $\Delta[\text{Fe}/\text{H}]$ between our inverted values and reference values, we find: HD 30508, 40 Eri and

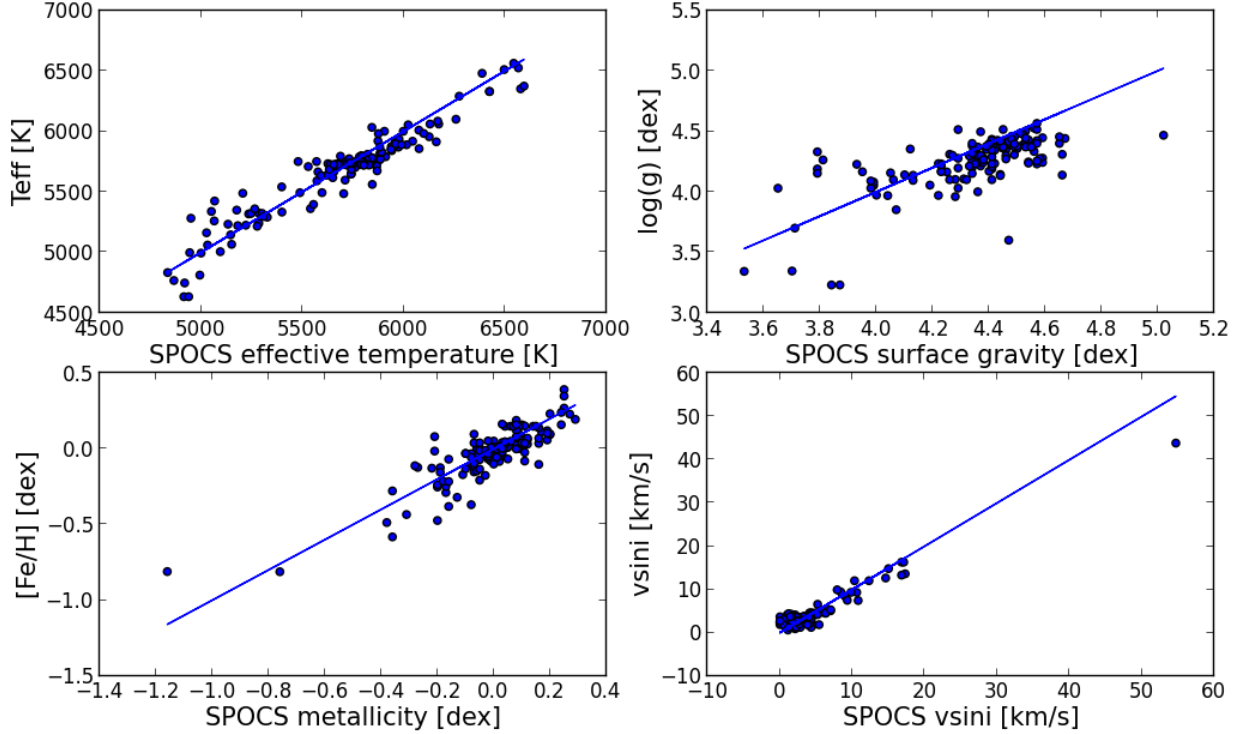


Fig. 7. Stellar fundamental parameters inverted from POLARBASE spectra in common with the SPOCS catalogue, using our PCA-Elodie method vs. SPOCS reference values, including $v\sin i$. Respective bias and standard deviation deduced from the analysis of the difference between inverted and reference parameters are: (23 ; 115) for T_{eff} , (0.10 ; 0.19) for $\log g$, (0.02 ; 0.10) for $[\text{Fe}/\text{H}]$, and (-0.04 ; 1.68) for $v\sin i$.

LHS 3976. We found systematically better agreement between our estimate and statistics on *all* data available at VizieR, to within 0.05 dex.

5.3.4. Projected rotational velocity

Our determinations of $v\sin i$ are correct and especially interesting for those objects having a significant projected rotational velocity, say greater than about 10 km s^{-1} . The major outlier, as seen in Fig (7), is HR 1817 for which we derive a $v\sin i \sim 43 \text{ km s}^{-1}$ while SPOCS value is about 55 km s^{-1} . It is a F8V RSCVn star aka. AF Lep for which another value of 52.6 km s^{-1} , still about 10 km s^{-1} greater than our estimate, was more recently published by Schroeder et al. (2009).

Concerning the determination of $v\sin i$, it is true that other methods of evaluation already exist. However, to the best of our knowledge, they require a template (synthetic) spectrum at $v\sin i \sim 0$ or, at least, a list of spectral lines *a priori* expected in the spectra, as auxiliary and “support” data (see e.g., Díaz et al. 2012 and references therein). Data processing tools that we shall attach further to POLARBASE will therefore include a complementary Fourier analysis module providing an additional $v\sin i$ determination, once stellar fundamental parameters will have been available from our inversion tool⁷. Note also that, with our PCA-based method, we are mostly interested in the “intermediate”

$v\sin i$ regime, say between 10 and 100 km s^{-1} . Indeed, for slower rotators for which rotational broadening becomes of the order of other sources of broadening (e.g., instrumental or turbulent), a more detailed or specific line profile analysis may be required.

6. Discussion

As briefly remarked earlier, the fact that the current implementation of our method relies on observed data makes it also somewhat relevant to *classification*. Indeed, we do not just identify “nearest spectra” since nearest neighbour(s) can also be identified as *objects* i.e., other stars. This important fact is also totally *independent* from whatever method of determination of stellar parameters have been used for these objects.

Therefore, unless modifying the sample of spectra/objects constituting our training database, we do not expect any change in the relation between inverted spectra and nearest neighbours *as objects*, even though evaluations of their various stellar parameters still may change in time. Another interesting point is that, this is also true for *any other stellar parameter* – especially those contributing to the spectral signature of a star, beyond the limited set of fundamental parameters we considered in this study.

Taking advantage of this, instead of using values given by the only Elodie catalogue, for each SPOCS spectra we analysed, we have gathered for every nearest neighbour *all* the evaluations of effective temperature, surface gravity and metallicity provided

⁷ The same is true for the refinement of radial velocity measurements which can be improved by “line addition” once identified a proper list of expected spectral line wavelengths (at rest).

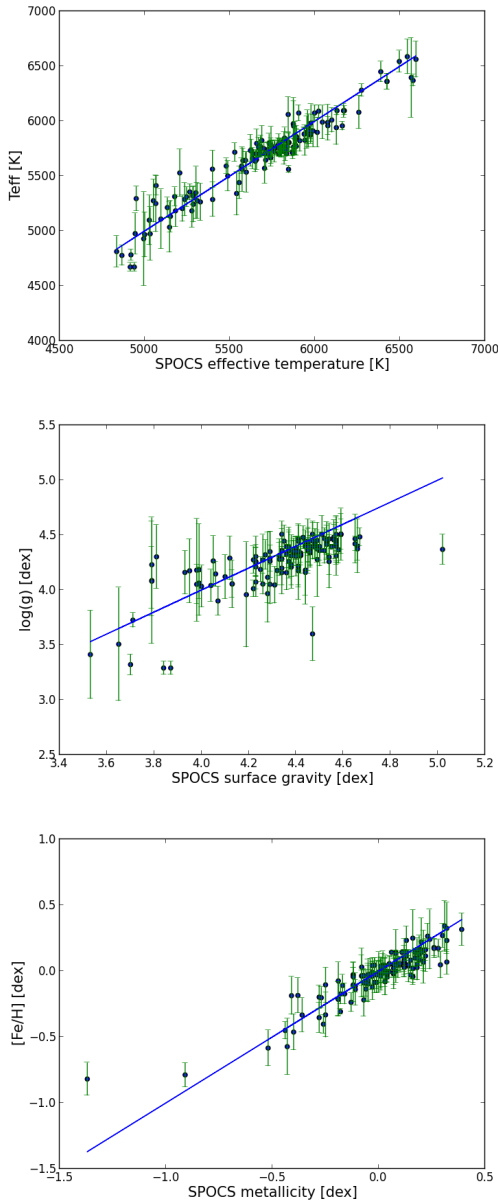


Fig. 8. Stellar fundamental parameters, and their respective uncertainties, inverted from POLARBASE spectra in common with the SPOCS catalogue, using our PCA-Elodie method vs. SPOCS reference values. These values were deduced from all determinations for each nearest neighbour compiled in the PASTEL catalogue of Soubiran et al. (2010).

by the comprehensive PASTEL catalogue⁸ (Soubiran et al. 2010). We could also evaluate uncertainties on each fundamental parameters as the standard deviation of the full set of collected values, except the unavailable projected rotational velocity though. Results are displayed in Figs. (8) and details are given in Table 5. Mean errors given in Table 5 are, respectively, 110 K, 0.16 dex and 0.09 dex for T_{eff} , $\log g$ and $[\text{Fe}/\text{H}]$ i.e., quite consistent, but slightly better than standard deviation values already given in Table 4.

⁸ For 4 targets for which we could not retrieve data from PASTEL, we used instead its TGMET values (Katz et al. 1998) also available from the Elodie@VizieR catalogue.

As a final remark, it is also worth mentioning that, although we used it together with a training database made of observed spectra, our PCA-based inversion method can be equally implemented using *synthetic* spectra.

7. Conclusion

We have implemented a fast and reliable PCA-based numerical method for the inversion of stellar fundamental parameters T_{eff} , $\log g$ and $[\text{Fe}/\text{H}]$, as well as the projected rotational velocity $v \sin i$, from the analysis of high-resolution Echelle spectra delivered by Narval and Espadons spectropolarimeters. First tests, mainly made with FGK-stars spectra, show good agreement between our inverted stellar parameters and reference values published by Allende Prieto et al. (2004) and Valenti & Fischer (2005). We also believe that our method will be efficient as well for the analysis of spectra from cooler M stars, as well as from hotter stars, up to spectral type A.

We used it, so far, with a spectral band located at the vicinity of the b-triplet of Mg I and without any help from additional (e.g., photometric) information, which is particularly challenging. However we can easily, either extend or change the spectral domain of use, or combine analyses from several distinct spectral domains, in order to constrain further and refine stellar parameters determination. In that respect, it is important to realize that PCA allows for a quite dramatic reduction of dimensionality, of the order of 800 ($\sim N_{\lambda}/k_{\text{max}}$) for the configuration we presented here. This capability is indeed of great interest for a comprehensive post-processing of high-resolution spectra covering a very large bandwidth like the ones from Espadons and Narval spectropolarimeters.

Acknowledgements. This research has made use of the VizieR catalogue access tool, CDS, Strasbourg, France. The original description of the VizieR service was published in A&AS 143, 23. This research has made use of the SIMBAD database, operated at CDS, Strasbourg, France. POLARBASE data were provided by the OV-GSO (ov-gso.irap.omp.eu) datacenter operated by CNRS/INSU and the *Université Paul Sabatier, Observatoire Midi-Pyrénées*, Toulouse (France).

References

- Allende Prieto, C., Barklem, P.S., Lambert, D.L., Cunha, K. 2004, A&A, 420, 183
 Bailer-Jones, C.A.L., Irwin, M., von Hippel, T. 1998, MNRAS, 298, 361
 Bailer-Jones, C.A.L. 2000, ApJ, 357, 197
 Cabanac, R.A., de Lapparent, V., Hickson, P. 2002, A&A, 389, 1090
 Casini, R., Asensio Ramos, A., Lites, B. W., López Ariste, A. 2013, ApJ, 773, 180
 Cayrel de Strobel, G. 1969, in Proceedings of the 3rd Harvard-Smithsonian Conference on Stellar Atmospheres, ed. O. Gingerich, 35
 Cayrel, G., Cayrel, R. 1963, ApJ, 137, 431
 Deeming, T.J. 1964, MNRAS, 127, 493
 Díaz, C.G., González, J.F., Levato, H., Grosso, M. 2011, A&A, 531, A143
 Gazzano, J.-C., de Laverny, P., Deleuil, M., et al. 2010, A&A, 523, 91
 Glebocki, R., Gnaniński, P. 2005 [2005yCat.3244...0G]
 Jones, M.I., Jenkins, J.S., Rojo, P., Melo, C.H.F. 2011, A&A, 536, 71
 Katz, D., Soubiran, C., Cayrel, R., Adda, M., Cautain, R. 1998, A&A, 338, 151
 Lee, Y.S., Beers, T.C., Allende Prieto, C., et al. 2011, AJ, 141, 90
 Maldonado, J., Eiroa, C., Villaver, E., Montesinos, B., Mora, A. 2012, A&A, 541, A40
 Massarotti, A., Latham, D.W., Stefanik, R.P., Fogel, J. 2008, AJ, 135, 209
 Molenda-Žakowicz, J., Sousa, S.G., Frasca, A., et al. 2013, MNRAS, 434, 1422
 Munari, U. 1999, Baltic Astron., 8, 73
 Munari, U., Sordo, R., Castelli, F., Zwitter, T. 2005, A&A, 442, 1127
 Muñoz Bermejo, J., Asensio Ramos, A., Allende Prieto, C. 2013, A&A, 553, 95
 Paletou, F. 2012, A&A, 544, 4
 Paletou, F., Zolotukhin, I. 2014 [arXiv:1408.7026]
 Petit, P., Louge, T., Théado, S., et al. 2014, PASP, 126, 469

- Porto de Mello, G. F., da Silva, R., da Silva, L., de Nader, R. V. 2014, *A&A*, 563, A52
- Prugniel, P., Soubiran, C. 2001, *A&A*, 369, 1048
- Prugniel, P., Soubiran, C., Koleva, M., Le Borgne D. 2007, [arXiv:astro-ph/0703658]
- Recio-Blanco, A., Bijaoui, A., de Laverny, P., et al. 2006, *MNRAS*, 370, 141
- Rees, D.E., López Ariste, A., Thatcher, J., Semel, M. 2000, *A&A*, 355, 759
- Re Fiorentin, P., Bailer-Jones, C.A.L., Lee, et al. 2007, *A&A*, 465, 1373
- Schröder, C., Reiners, A., Schmitt, J.H.M.M. 2009, *A&A*, 493, 1099
- Semel, M., Donati, J.F., Rees, D.E. 1993, *A&A*, 278, 231
- Soubiran, C., Le Campion, J.-F., Cayrel de Strobel, G., Caillo, A. 2010, *A&A*, 515, 111
- Tucci Maia, M., Meléndez, J., Ramírez, I. 2014, *ApJ*, 790, L25
- Valenti, J.A., Fischer, D.A. 2005, *ApJS*, 159, 141

Table 5. Values and respective uncertainties of the inverted stellar parameters T_{eff} , $\log g$ and $[\text{Fe}/\text{H}]$ for SPOCS objects in common with POLARBASE using our Elodie based PCA method.

Object	T_{eff} [K]	$\sigma_{T_{\text{eff}}}$ [K]	$\log g$ [dex]	$\sigma_{\log g}$ [dex]	$[\text{Fe}/\text{H}]$ [dex]	$\sigma_{[\text{Fe}/\text{H}]}$ [dex]
HR753	4777	91	4.40	0.24	-0.03	0.09
LTT11292	5562	203	4.46	0.14	-0.02	0.11
39Tau	5763	75	4.36	0.12	0.05	0.06
LTT11169	5098	226	3.51	0.52	-0.10	0.13
LTT11282	5990	153	4.21	0.20	0.04	0.10
109Psc	5768	100	4.29	0.20	0.17	0.10
107Psc	5183	145	4.45	0.17	-0.03	0.12
LHS5051a	5645	86	4.40	0.03	0.13	0.03
HD12846	5734	100	4.31	0.16	-0.20	0.09
LTT10989	5702	19	4.39	0.02	0.14	0.01
13Tri	5854	77	3.90	0.13	-0.24	0.07
HD30825	5312	85	3.73	0.07	-0.11	0.08
LHS1753	5821	98	4.26	0.15	0.03	0.07
G175-33	5724	120	4.21	0.17	0.23	0.09
HD9472	5718	39	4.48	0.08	-0.00	0.05
V*V451And	5732	144	4.47	0.10	-0.00	0.08
LTT10580	5702	19	4.39	0.02	0.14	0.01
LHS1125	4974	242	4.51	0.14	0.05	0.12
HD5065	5945	154	4.05	0.22	-0.10	0.14
etaCas	5825	140	4.18	0.23	-0.33	0.17
LTT11104	6369	53	3.97	0.09	0.08	0.06
V*V987Cas	5264	168	4.46	0.14	0.00	0.12
G245-27	5649	91	4.42	0.14	0.04	0.09
HD73344	6095	41	4.18	0.13	0.11	0.04
55Cnc	5287	151	4.43	0.09	0.34	0.19
LTT12401	5897	134	4.30	0.16	-0.00	0.09
HR3499	6080	150	4.18	0.27	0.04	0.12
24LMi	5768	83	4.26	0.13	0.05	0.05
LHS2216	5749	50	4.35	0.18	0.16	0.06
HR4486	5840	154	4.36	0.17	-0.21	0.13
36UMa	5940	156	4.20	0.24	-0.22	0.12
HD98618	5773	57	4.34	0.11	0.04	0.05
V*V377Gem	5781	168	4.48	0.07	-0.02	0.08
NLTT17627	5804	86	4.34	0.12	-0.01	0.09
LTT12204	5822	81	4.34	0.13	-0.02	0.07
HD71881	5845	96	4.26	0.15	-0.03	0.08
HD138573	5739	65	4.36	0.11	0.04	0.06
HR5659	5702	19	4.39	0.02	0.14	0.01
GJ566A	5591	69	4.42	0.07	-0.03	0.04
HD129814	5808	88	4.31	0.13	-0.01	0.08
tauBoo	6449	93	4.27	0.23	0.26	0.10
sigBoo	6396	362	3.96	0.48	-0.57	0.21
LHS348	5987	163	4.31	0.18	0.05	0.09
LHS2498	5275	195	4.09	0.57	-0.19	0.13
V*EKDra	5561	32	3.60	0.24	-0.04	0.02
V*HN Peg	5872	78	4.51	0.12	-0.09	0.08
HR8455	5796	129	4.17	0.29	-0.11	0.13
V*V376Peg	6009	112	4.23	0.21	-0.04	0.11
HD195019	5787	96	4.25	0.13	0.05	0.07
LTT16813	5341	198	4.40	0.25	0.07	0.16
V*V454And	5710	54	4.44	0.13	0.08	0.08
HR8832	4812	142	4.46	0.18	0.10	0.15
LHS544	5213	92	4.39	0.19	0.00	0.10
LTT15779	5770	69	4.32	0.12	0.06	0.05
LTT15881	5702	19	4.39	0.02	0.14	0.01
LTT16028	5805	33	4.39	0.15	-0.11	0.05
HD173701	5286	156	4.43	0.10	0.32	0.20
HR7294	5745	70	4.36	0.10	0.04	0.06

Table 5. continued.

Object	T_{eff} [K]	$\sigma_{T_{\text{eff}}}$ [K]	$\log g$ [dex]	$\sigma_{\log g}$ [dex]	[Fe/H] [dex]	$\sigma_{[\text{Fe}/\text{H}]}$ [dex]
LTT15729	6562	164	4.04	0.14	-0.04	0.16
16CygB	5776	70	4.28	0.11	0.06	0.05
sigDra	5310	89	4.45	0.14	-0.07	0.14
LTT149	5754	62	4.33	0.16	0.16	0.09
LHS146	5319	81	4.51	0.24	-0.58	0.14
HD12328	4782	50	3.32	0.09	0.05	0.10
HR448	5881	57	4.06	0.12	0.18	0.07
LTT1267	5778	64	4.27	0.12	0.10	0.07
HD3821	5738	98	4.36	0.13	-0.14	0.10
G270-82	5634	98	4.40	0.15	-0.21	0.13
LTT709	6090	57	4.19	0.11	0.05	0.06
LTT10409	5412	90	4.30	0.29	-0.19	0.14
HR222	4976	186	4.51	0.17	-0.20	0.08
HD9986	5744	66	4.36	0.11	0.04	0.06
LTT8887	5440	148	4.28	0.34	0.15	0.15
LTT9062	5764	87	4.32	0.15	-0.03	0.10
HR8931	5884	47	4.05	0.17	-0.40	0.07
G157-8	5897	147	4.29	0.24	-0.14	0.12
HR8734	5570	137	4.26	0.24	0.32	0.12
LTT8785	4672	38	3.29	0.06	-0.05	0.05
HD208776	5981	172	4.03	0.19	-0.07	0.16
HD377	5975	236	4.12	0.41	-0.03	0.03
LHS1239	5724	99	4.35	0.14	-0.17	0.08
G131-59	5799	86	4.32	0.13	-0.01	0.09
54Psc	5204	119	4.36	0.19	0.02	0.12
HD218687	6073	72	4.45	0.14	-0.04	0.04
LTT16778	5348	238	4.18	0.42	0.22	0.18
V*MT Peg	5783	88	4.36	0.14	0.02	0.07
51 Peg	5702	19	4.39	0.02	0.14	0.01
G131-18	5355	72	4.51	0.18	-0.45	0.07
V*V439 And	5640	110	4.37	0.12	0.03	0.09
V*V344 And	5660	96	4.37	0.10	0.07	0.09
LHS3976	5666	79	4.31	0.18	-0.46	0.14
V*AF Lep	6542	99	4.37	0.14	0.05	0.10
HR2622	5957	81	4.05	0.09	0.09	0.05
HD46375	5243	164	4.42	0.13	0.24	0.23
alf CMi	6587	157	4.06	0.14	-0.01	0.15
LTT2093	5882	60	4.07	0.13	0.17	0.07
40 Eri	5133	142	4.45	0.22	-0.35	0.11
HD30508	5528	215	4.08	0.32	0.03	0.14
HR1232	4928	426	3.41	0.40	0.11	0.12
LTT1723	5249	258	4.23	0.40	0.13	0.18
LHS1577	5823	134	4.22	0.19	-0.79	0.09
HD22918	4672	38	3.29	0.06	-0.05	0.05
V*kap01 Cet	5745	101	4.45	0.09	0.08	0.11
1 Ori	6361	73	4.05	0.18	-0.08	0.10
HR2251	5857	99	4.28	0.15	-0.02	0.08
LTT11933	5911	151	4.35	0.20	-0.09	0.10
37 Gem	5770	82	4.16	0.16	-0.31	0.02
V*chi01 Ori	5872	78	4.51	0.12	-0.09	0.08
LTT5873	5275	164	4.46	0.14	-0.01	0.11
LTT3686	5702	19	4.39	0.02	0.14	0.01
LHS2465	5956	40	4.01	0.07	0.10	0.03
LTT12723	5751	67	4.38	0.10	0.04	0.05
17 Vir	6095	41	4.18	0.13	0.11	0.04
V*LW Com	5702	19	4.39	0.02	0.14	0.01
LTT13145	5910	146	4.31	0.19	-0.03	0.11
LTT13442	6281	57	4.15	0.11	0.17	0.07
61 UMa	5500	137	4.48	0.10	-0.04	0.10
LHS44	5294	112	4.47	0.22	-0.82	0.12
LTT7713	5762	61	4.32	0.07	0.06	0.05

Table 5. continued.

Object	T_{eff} [K]	$\sigma_{T_{\text{eff}}}$ [K]	$\log g$ [dex]	$\sigma_{\log g}$ [dex]	[Fe/H] [dex]	$\sigma_{[\text{Fe}/\text{H}]}$ [dex]
HD175726	6073	72	4.45	0.14	-0.04	0.04
18Sco	5752	75	4.35	0.13	0.04	0.06
V*V2133Oph	5183	150	4.44	0.18	-0.02	0.12
V*V2292Oph	5591	69	4.42	0.07	-0.03	0.04
HD169822	5643	73	4.44	0.10	-0.04	0.07
HD159909	5733	73	4.35	0.13	0.08	0.08
HR6950	5562	169	4.16	0.20	0.23	0.11
110Her	6361	73	4.05	0.18	-0.08	0.10
LTT15317	5747	77	4.40	0.13	-0.09	0.10
HD166435	6060	160	4.16	0.29	-0.02	0.07
86Her	5535	184	4.12	0.20	0.27	0.09
HR6806	4966	205	4.45	0.17	-0.17	0.08
V*delEri	5108	270	4.18	0.47	0.25	0.21
V*epsEri	5034	228	4.51	0.16	-0.12	0.10
LTT1601	5716	84	4.26	0.23	-0.33	0.13
LHS1845	5748	70	4.35	0.10	0.04	0.06
V*V401Hya	5746	63	4.39	0.11	0.08	0.08
LTT3283	5702	19	4.39	0.02	0.14	0.01
HD145825	5742	71	4.37	0.12	0.04	0.06
HD143006	5956	227	4.30	0.18	0.16	0.08
HR7291	6094	60	4.16	0.11	0.05	0.07